Interfacial Instability of a Non-magnetized Drop in Ferrofluids Subjected to an Azimuthal Field: A Diffuse-Interface Approach

Ching-Yao Chen and Ting-Shiang Lin

Abstract We perform direct numerical simulations of a non-magnetic drop immersed in immiscible ferrofluids in a confined Hele-Shaw cell under an azimuthal field by a diffuse-interface method. The interface is unstable in such a condition because of the inward attraction of the ferrofluids induced by the magnetic field gradient. We focus on the fingering onset and pattern influenced by the coupling viscous effect with different viscously stable conditions, which is achieved by varying the viscosity contrast of the ferrofluids and non-magnetic drop. In a viscously stable condition, in which the viscosity of the ferrofluids is greater than the immersed drop, the fingering onset takes place earlier because of the higher mobility of drop. The fingering pattern is simpler with numerous straightly developed fingers. On the other hand, a viscously unstable interface of less viscous ferrofluids results in ramified fingering pattern associated with the secondary phenomena, e.g., competitions and tip-splits of fingers. However, the fingering onset is delayed because the drop is less mobile.

1 Introduction

Ferrofluids conveniently combine the fluidity of liquids and the magnetic properties of solids. They are stable colloidal suspensions of magnetic nano-particles suspended in a non-magnetic carrier fluid, which has been a fascinating field of research for several decades [1, 2]. The pronounced superparamagnetic property of ferrofluids allows distant manipulation of their flow and interfacial behavior with external magnetic fields. Consequently, the phenomena of interfacial pattern formation in ferrofluids has received considerable attention. One striking example of pattern-forming systems in ferrofluids is the famous Rosensweig instability [3–7] in a uniform perpendicular field to an initially flat, ferrofluid free surface, which leads to the development of 3-dimensional hexagonal array of peaks. Another type of

C.-Y. Chen (✉) • T.-S. Lin
Department of Mechanical Engineering, National Chiao Tung University, Hsinchu, Taiwan 30010, R.O.C.
e-mail: chingyao@mail.nctu.edu.tw

Y. Bazilevs, K. Takizawa (eds.), *Advances in Computational Fluid-Structure Interaction and Flow Simulation*, Modeling and Simulation in Science, Engineering and Technology, DOI 10.1007/978-3-319-40827-9_14

remarkable patterns is associated with the so-called labyrinthine instability [8–13], where highly branched structures are formed when a ferrofluid droplet is trapped in the effectively 2-dimensional configuration of a Hele-Shaw cell [14] under a perpendicular uniform magnetic field. These two instabilities can co-exist to form a new hybrid instability if the confining upper plate of the Hele-Shaw cell is replaced by a free fluid surface [15]. Besides the two well-known interfacial instabilities under a uniform field, a non-uniform azimuthal field has also been demonstrated to stabilize a rotating heavier ferrofluid droplet surrounded by non-magnetic fluids, in which the interfacial instability is triggered by the centrifugal forces [16, 17]. This stabilizing effect is expected to reverse if an azimuthal field is applied to a non-magnetic drop immersed in ferrofluids, which is confirmed by a recent theoretical analysis [18]. In this paper we perform direct numerical simulations of this de-stabilizing effect by a highly accurate diffuse-interface method. In this context, our aim is to consider the coupling between capillary force and magnetic effects, and study how they give rise to still unexplored interfacial shapes and interesting dynamical behaviors.

2 Physical Problem and Governing Equations

We investigate the interfacial instability of a circular non-magnetized drop (fluid 2) with an initial radius R_0 surrounded by immiscible ferrofluids (fluid 1) in a Hele-Shaw cell, as the principle sketch shown in Fig. 1. The Hele-Shaw cell has gap spacing h. An azimuthal magnetic field $\mathbf{H}$ is generated by a wire carrying electric current strength I placed at the center of the drop. The viscosities of ferrofluids and the non-magnetic drop are denoted by η_1 and η_2, respectively. We focus on the magneto-induced motion, but allow the inner drop to be either more or less viscous than the outer ferrofluids. The governing equations of such an immiscible interface approached by diffuse-interface method are based on the model proposed by Cahn and Hilliard [19]. In the context of a Hele-Shaw cell system [20–25] incorporating with magnetic stress [16–18], the equations can be written as

$$\frac{\partial \rho}{\partial t} + \nabla \cdot (\rho \mathbf{u}) = 0, \tag{1}$$

$$\nabla p = -\frac{12\eta}{h^2}\mathbf{u} + \mu_0 M \nabla H - \epsilon \nabla \cdot [\rho(\nabla c)(\nabla c)^T], \tag{2}$$

$$\rho\left(\frac{\partial c}{\partial t} + \mathbf{u}\cdot\nabla c\right) = \alpha \nabla^2 \mu, \tag{3}$$

$$\mu = \frac{\partial f_0}{\partial c} - \frac{\epsilon}{\rho}\nabla \cdot (\rho \nabla c) - \frac{p}{\rho^2}\frac{d\rho}{dc}, \tag{4}$$

$$f_0 = f^* c^2 (1-c)^2. \tag{5}$$

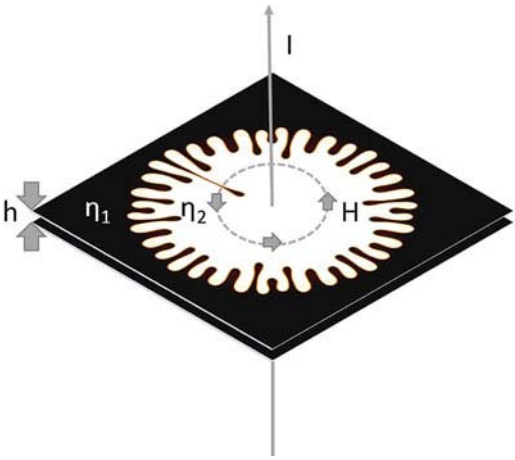

Fig. 1 A non-magnetized drop (bright color) inside ferrofluids (dark color) confined in a Hele-Shaw cell with width h subjected to an azimuthal field H generated by a current-carrying (strength I) wire.

Here, $\mathbf{u}$ denotes the fluid velocity vector and p the pressure. The viscosity and the density of the binary fluid system are represented by η and ρ, respectively. The phase-field variable is represented by c, so that $c = 1$ in the ferrofluid, and $c = 0$ in the drop. μ_0, M, and H are the permeability in vacuum, magnitudes of magnetization, and field strength, respectively. The coefficients of capillarity and mobility are denoted by ϵ and α. The chemical potential is denoted by μ, and f_0 is a free energy (or, the Helmholtz free energy) with a characteristic specific energy f^*. Equations (1)–(5) define the so-called Hele-Shaw-Cahn-Hilliard (HSCH) model [20–25], and result in a surface free energy given by

$$E = \rho \int \left(f_0 + \frac{\epsilon}{2} (\nabla c)^2 \right) dV, \tag{6}$$

where V is the volume of the fluid domain.

The magnetic field $\mathbf{H}$ generated by a wire with electric current I perpendicular to the cell is expressed by [16–18]

$$\mathbf{H} = \frac{I}{2\pi r} \mathbf{e}_{\boldsymbol{\theta}}, \tag{7}$$

where r is the radial position, and $\mathbf{e}_{\boldsymbol{\theta}}$ represents the unit vector along the azimuthal direction. A proportional magnetization strength of the ferrofluids to the field associated with a constant susceptibility χ can be approximated, so that

$$\mathbf{M}(c) = \chi \mathbf{H} c. \tag{8}$$

A correlation of viscosity (η) with the phase-field variable c is are required by the present approach. To take advantage of the highly accurate scheme previously developed for Hele-Shaw flows [26–28], we assume that

$$\eta(c) = \eta_1 e^{[R(1-c)]},\ R = \ln\left(\frac{\eta_2}{\eta_1}\right). \tag{9}$$

Here, R is the logarithmic viscosity contrast parameter. We further assume the flow incompressible, so that density ρ is constant. In order to render the governing equations dimensionless, the initial radius of the fluid drop R_0 and viscosity of ferrofluid η_1 are taken as characteristic scales. In conjunction with a characteristic velocity $\mu_0 h^2 I^2/48\eta_1\pi^2 R_0^3$, a characteristic pressure $\mu_0 I^2/4\pi^2 R_0^2$, and a characteristic specific free energy ${f_0}^*$, the dimensionless HSCH equations associated with Eq. (1)–(5) can be written as

$$\nabla \cdot \mathbf{u} = 0, \tag{10}$$

$$\nabla p = -\eta\mathbf{u} - \frac{\chi c}{r}\nabla\left(\frac{1}{r}\right) - \frac{C}{Mg}\nabla \cdot [(\nabla c)(\nabla c)^T], \tag{11}$$

$$\frac{\partial c}{\partial t} + \mathbf{u}\cdot\nabla c = \frac{1}{\mathrm{Pe}}\nabla^2\mu, \tag{12}$$

$$\mu = \frac{\partial f_0}{\partial c} - C\nabla^2 c, \tag{13}$$

$$f_0 = c^2(1-c)^2. \tag{14}$$

Dimensionless parameters, such as the Peclet number Pe, the Atwood number (normalized viscosity contrast) A, the Cahn number C, and magnetic strength Mg, are defined as

$$\mathrm{Pe} = \frac{\mu_0 h^2 I^2}{48\pi^2\alpha\eta_1 f^* R_0^2},\ A = \frac{e^R - 1}{e^R + 1},\ C = \frac{\epsilon}{f^* R_0^2},\ \mathrm{Mg} = \frac{\mu_0 I^2}{4\pi^2\rho f^* R_0^2}.$$

Moreover, the dimensionless free interfacial energy corresponding to Eq. (6) can be obtained accordingly as

$$E = \frac{1}{\mathrm{Mg}}\int\left(f_0 + \frac{C}{2}(\nabla c)^2\right)dV. \tag{15}$$

In order to solve the governing equations numerically, we recast the governing equations into the well-known streamfunction-vorticity formulation (ϕ, ω) [26], yielding

$$u = \frac{\partial\phi}{\partial y},\ v = -\frac{\partial\phi}{\partial x} \tag{16}$$

$$\nabla^2\phi = -\omega, \tag{17}$$

where

$$\omega = -R\left(u\frac{\partial c}{\partial y} - v\frac{\partial c}{\partial x}\right) - \frac{\chi}{\eta r^4}\left(y\frac{\partial c}{\partial x} - x\frac{\partial c}{\partial y}\right) + \frac{C}{\eta \mathrm{Mg}}\left[\frac{\partial c}{\partial x}\left(\frac{\partial^3 c}{\partial x^2 \partial y} + \frac{\partial^3 c}{\partial y^3}\right) - \frac{\partial c}{\partial y}\left(\frac{\partial^3 c}{\partial x \partial y^2} + \frac{\partial^3 c}{\partial x^3}\right)\right].$$

Boundary conditions are prescribed as follows:

$$x = \pm 1 \ : \phi = 0, \ \frac{\partial c}{\partial x} = 0, \ \frac{\partial^2 c}{\partial x^2} = 0, \tag{18}$$

$$y = \pm 1 \ : \ \phi = 0, \ \frac{\partial c}{\partial y} = 0, \ \frac{\partial^2 c}{\partial y^2} = 0. \tag{19}$$

To reproduce the extremely fine structures of the fingers, a highly accurate pseudospectral method is employed. As a result, the actual boundary conditions applied in the numerical code are $\partial\phi/\partial y = 0$ at $y = \pm 1$. However, at the present situation where no concentration gradient is generated on the boundaries, the above conditions automatically lead to $\phi = 0$. To ensure this condition, all the simulations are terminated when the inner fluid reaches a certain distance away from the computational boundaries. Both c and ϕ are expanded in a cosine series in the x-direction. In the y-direction, discretization is accomplished by sixth order compact finite differences. Time integration is fully explicit and utilizes a third order Runge–Kutta procedure. The evaluation of the nonlinearity at each time level is performed in a pseudospectral manner. The procedures reported in Refs. [23–25] are followed, in which $Pe = 3000$ and $C = 10^{-5}$ are applied to approach an immiscible interface. The simulations are terminated when the fastest penetrating fingers reach near the origin to avoid numerical instability. For a more detailed account about these numerical schemes the reader is referred to Refs. [23–28].

3 Numerical Results and Discussion

In the following simulations, we present the fingering patterns induced by the destabilizing magnetic field. Influences of the magnetic effects, e.g., the magnetic strength Mg and the magnetic susceptibility χ, coupled with the viscosity contrast A will be analyzed systematically. It is noticed that a positive/negative A represents more/less viscous non-magnetic drop than the surrounding ferrofluids, respectively. For the case of $A = 0$, the drop and ferrofluids are with the same viscosity.

Shown in Fig. 2 are three representative cases for $Mg = 2$ and $\chi = 1$ for various viscosity contrast $A = -0.462$, 0, and 0.462. The presence of magnetic field gradient triggered vigorous fingering instability. The negative radial field gradient attracts the ferrofluids to penetrate into the drop toward the origin, and

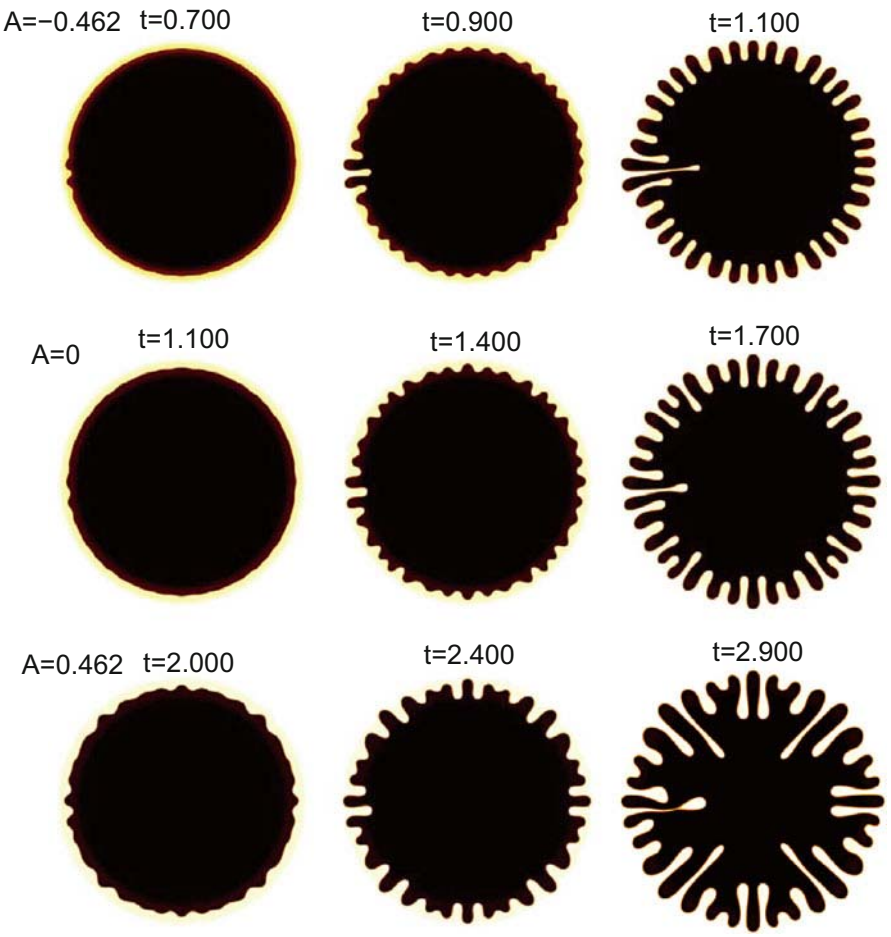

Fig. 2 Fingering patterns for $A = -0.462$ [top row], $A = 0$ [middle row], and $A = 0.462$ [bottom row]. The remaining parameters are: Mg=2 and $\chi = 1$. For better observation of the interfacial instability, the non-magnetic drop is shown by dark color in the present figures. The left, middle, and right columns show the patterns of (1) immediately after the emergences of fingers, (2) fully developed fingers, and (3) shortly before the most inward finger reaching the core, respectively.

squeeze partial mass of the drop to stretch outwardly. For easier identification, the penetrating ferrofluid fingers and stretching fingers of non-magnetic drop are denoted as inward fingers and outward fingers, respectively. For various Atwood numbers, the fingering patterns show apparent distinctions. For a negative Atwood number of $A = -0.462$ as the fingering pattern shown in the top row of Fig. 2, in which the viscosity of non-magnetic drop is smaller than the ferrofluids, the fingering pattern is very regular without strong finger competition, i.e., most of the fingers emerging compatibly. Both the outward and inward fingers develop in a nearly identical path to preserve circular inward and outward fingering fronts.

Nevertheless, because extremely significant field gradient near the origin as shown in Eq. (7), a few dominant fingers eventually emerge to reach the origin. Noted that the emergences of a few faster dominant fingers are similar to the fingering patterns of radial suction flow [24]. On the other hand, if the viscosity of the drop is increased to match the ferrofluids as the case of $A = 0$ shown in the middle row of Fig. 2, the fingering instability is enhanced. Some tips of outward fingers are seen to emerge secondary instability, e.g., fingertip split. The circular inward fingering front is no longer preserved, which indicates apparent fingering competition. If the viscosity of the drop is further increased to outmatch the ferrofluids, e.g., $A = 0.462$ as the pattern shown in the bottom row of Fig. 2, fingering competitions of the inward fingers and tip-split of the outward fingers are very prominent. The fingering patterns appear very different with variation of the viscosity contrast. These distinct fingering patterns can be realized by the underlining mechanism of well-developed viscous fingering phenomena. For the case of a negative $A = -0.462$, the interface is viscously stable, in which a more viscous ferrofluids penetrating (or displacing) a less viscous drop. The fingering pattern of viscously stable condition usually appears less fingering competition associated with a nearly circular fingering front as demonstrated in similar fingering patterns driven by centrifugal forces [23]. On the contrary, the less viscous ferrofluids penetrate inwardly into the more viscous drop in a positive $A = 0.462$, which is the typical instability of viscous fingering, so that the emergences of inward fingers appear very prominent with active secondary phenomena, e.g., fingering competitions and tip-split. As a result, the coupling effects of viscosity contrast with the de-stabilizing magnetic force can lead to entirely distinct patterns of interfacial instability. These coupling effects can be further enhanced by increasing the absolute magnitude of viscosity contrast to $A = -0.635$ and 0.635, as their fingering patterns shown in Fig. 3. The inward fingering competitions and outward tip-split are seen more prominent for these cases with stronger viscous influences.

As discussed in the previous paragraph, the fingering patters depend strongly on the viscous effect. It is also worthy to observe the onset and evolution of the fingering instability. The onset times of finger emergences for various Atwood numbers are shown in the left column of Figs. 2 and 3. It is interesting to discover that the onset of fingers occurs earlier for the condition, in which the ferrofluid is more viscous than the drop, e.g., onset at $t = 0.5, 0.7, 1.1, 2.0$, and 2.3 for $A = -0.635, -0.462, 0, 0.462$, and 0.635, respectively. The delay of fingering onset for less viscous ferrofluids penetrating into more viscous drop, in which the fingering pattern is more ramified as the fully evolved patterns shown in the middle and right columns of Figs. 2 and 3, suggests a contradict behavior in the measure of instability prominence. Considering the driven fluids are the ferrofluids, it is much easier for more viscous ferrofluids to displace the stationary less viscous drop whose mobility is higher. Consequently, the fingering onset occurs at earlier time. Nevertheless, since the interface is viscously stable, the fingering pattern appears simpler with primary straight inward fingers. On the contrary, it takes longer time to drive less viscous ferrofluids penetrating into the more viscous drop with less mobility. Afterward, the viscously unstable interface starts to evolve those

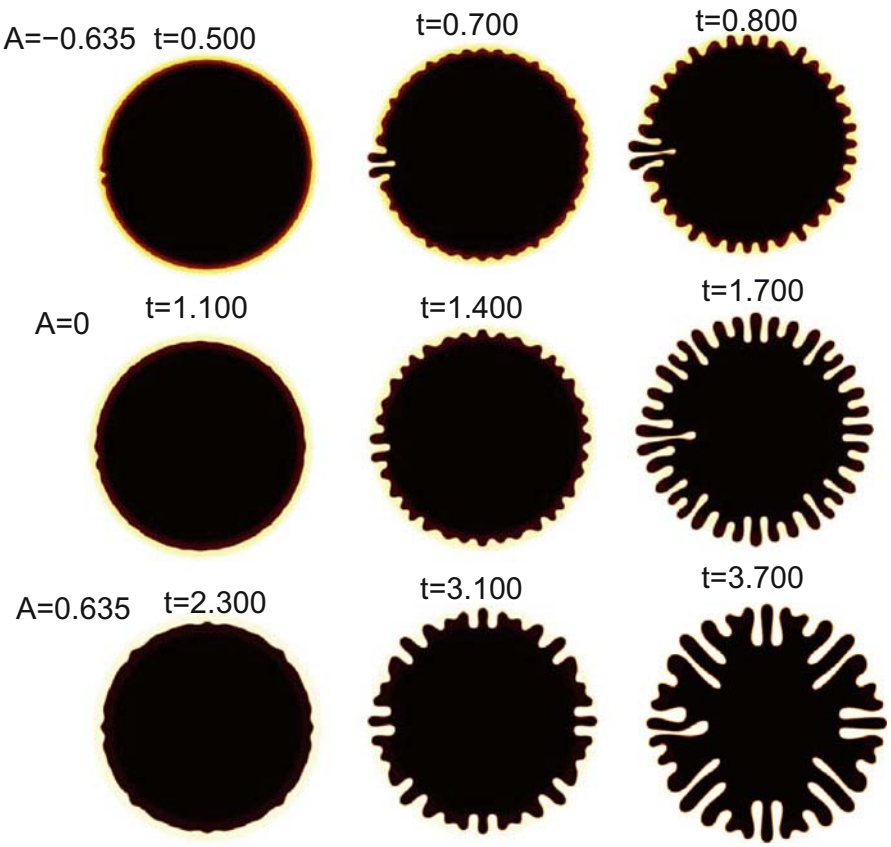

Fig. 3 Fingering patterns for $A = -0.635$ [top row], $A = 0$ [middle row], and $A = 0.635$ [bottom row]. The remaining parameters are: Mg=2 and $\chi = 1$.

secondary fingering phenomena and form more ramified pattern. As a result, the onset and pattern of fingering instability shows opposite trend with the viscosity contrast.

The effect of magnetic field is straightforward, such that stronger field strength shortens the onset of fingering instability, and results in a more vigorous fingering pattern. Quantitative measures will be presented in a latter paragraph. In Fig. 4, we show the patterns of $Mg = 4$ and $\chi = 0.5$ for $A = -0.635, 0$, and 0.635. It is noticed that they can be directly compared with the patterns shown in Fig. 3 with identical value of product for $\chi Mg = 2$. By the present dimensionless scaling, the main difference between Figs. 3 and 4 is the model dissipation. In general, even the evolution of the fingers is slower to allow longer simulating time period, the overall patterns show resemblances, e.g., same number of emerging fingers for $A = -0.635$ and similar fingering patterns for $A = 0.635$. These observations confirm that the model dissipation does not alter fingering patters significantly.

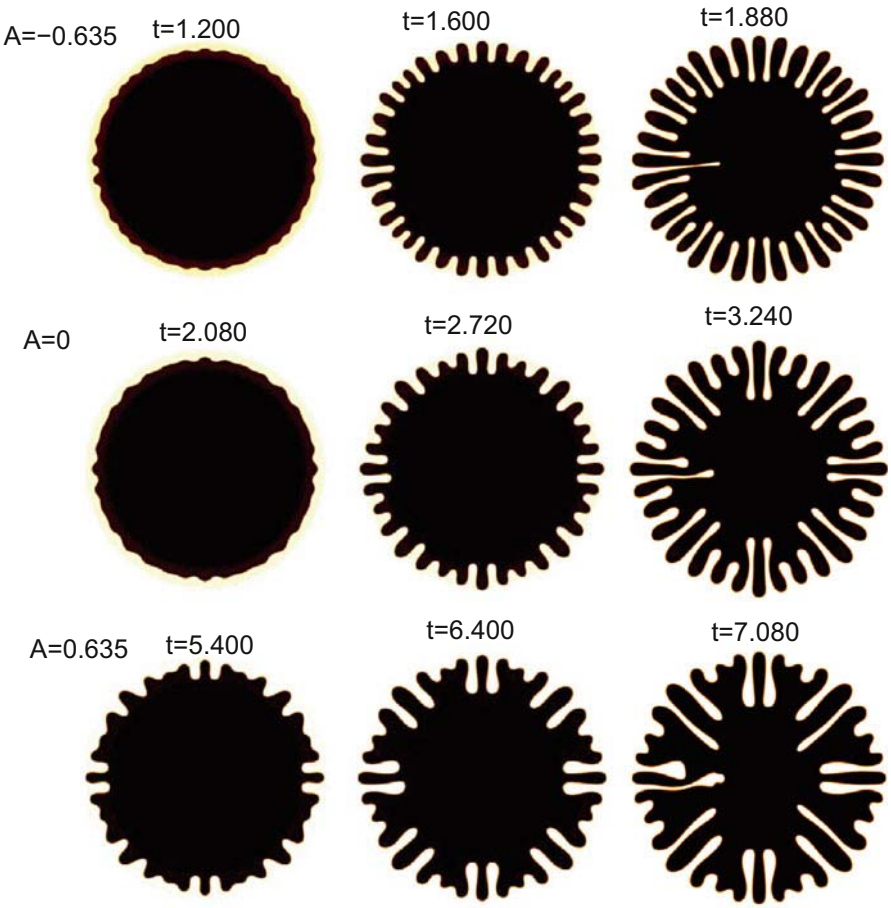

Fig. 4 Fingering patterns for $A = -0.635$ [top row], $A = 0$ [middle row], and $A = 0.635$ [bottom row]. The remaining parameters are: Mg=4 and $\chi = 0.5$.

To conclude this section, a quantitative measure of interfacial length L, which is capable to represent the prominence of the fingering instability, is presented for various control parameters. The interfacial length is approximated as [5]:

$$L_n(t) = \int_x \int_y \sqrt{(\frac{\partial c}{\partial x})^2 + (\frac{\partial c}{\partial y})^2} dxdy. \tag{20}$$

The fingering onset can be clearly identified at the time when the interfacial length starts to deviate from the base value of circular shape as shown in Fig. 5. In addition, longer interfacial length generally indicates more vigorous fingering pattern. In line with the earlier discussion, earlier fingering onset occurs for the cases of less

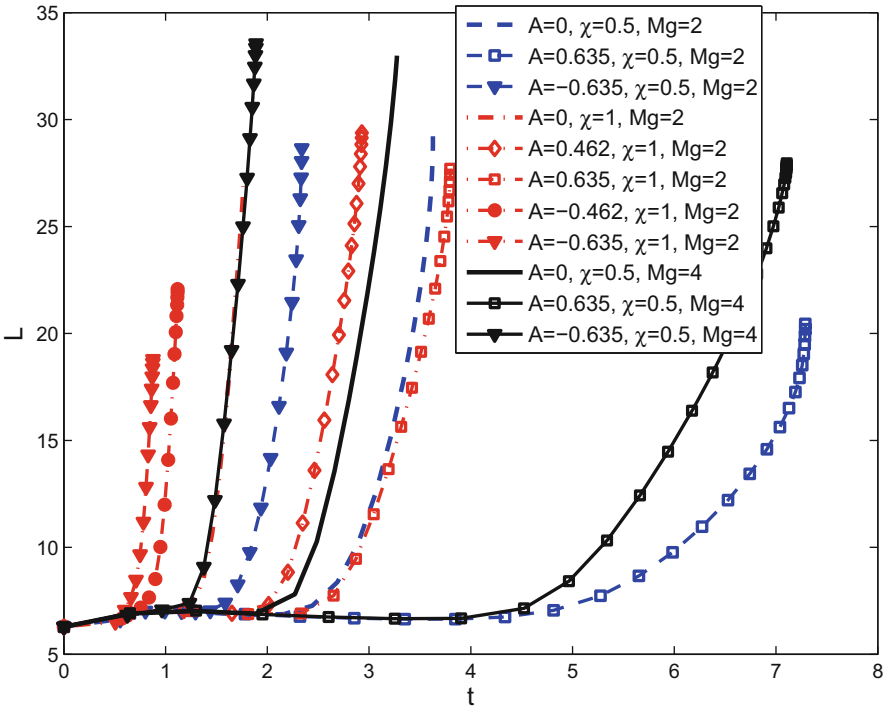

Fig. 5 Interfacial lengths for various parameters. Faster growth of interfacial length generally represents more unstable instability. Interfacial instability is in favor of the conditions with negative viscosity contrast and stronger magnetic effect.

viscous drop (negative A), stronger magnetic effect (higher Mg or χ). Nevertheless, the results for interfacial length appear contradictory. For $Mg = 2$ and $\chi = 0.5$, longer interfacial length at terminated simulating time is observed in the case of $A = -0.635$, which is viscously stable. Nevertheless, opposite results are found for case of $Mg = 2$ and $\chi = 1$, in which longer interfacial length appears for $A = 0.635$. This contradict behavior is resulted from the competitions of earlier fingering onset for a negative A and vigorous fingering pattern for a positive A. On the one hand, the interfacial length starts to growth after the onset time. On the other hand, the secondary fingering formation intensifies the growth of interfacial length. As a result, it leads to inconsistency to solely consider the interfacial length at the terminated time. Instead, it is more appropriate to consider the growth rate. All the cases clearly show higher growth rates of the interfacial lengths right before the terminated time for positive A, which indicates intensified secondary fingering behaviors in viscously unstable conditions.

4 Concluding Remarks

Direct numerical simulations of the interfacial instability of a non-magnetic drop surrounded by immiscible ferrofluids, confined in a Hele-Shaw cell, and subjected to an azimuthal field, are performed by a diffuse-interface method incorporating with highly accurate numerical schemes. The interface is unstable because of the inward attraction of the ferrofluids induced by the magnetic field gradient. The onset and pattern of interfacial fingering instability is analyzed to realize the coupling effects of the magnetic force and viscous contrast. If viscosity of the ferrofluids is greater than the immersed drop, in which the interface is viscously stable, the fingering onset takes place earlier because of the higher mobility of penetrated drop fluid. Nevertheless, the fingering pattern appears simpler with straightly emerging fingers. On the other hand, the viscously unstable interface, i.e., less viscous ferrofluids penetrating more viscous drop, results in more ramified pattern associated with the secondary fingering phenomena, e.g., competitions and tip-splits of fingers. However, the onset is delayed because less mobile drop fluid.

To quantify the prominence of fingering instability, development of the interfacial length is calculated as a global measure. In general, longer interfacial length indicates more unstable interface. We confirm the occurrences of earlier fingering onset and vigorous secondary phenomena both enhance growth of the interfacial length. Nevertheless, these two behaviors are favorable in opposite conditions, i.e., earlier onset and secondary phenomena in condition of more and less viscous ferrofluids, respectively, so that inconsistent evolutions of the interfacial length are observed. As a result, instead of the interfacial length, its growth rate is more appropriate for the consideration of the measure of instability. The earlier onset for cases of more viscous ferrofluids usually leads to greater growth rate in the early envelopment of fingering instability. On the contrary, the growth rate is dramatically enhanced at the later period when the secondary fingering phenomena are active for conditions of less viscous ferrofluids.

Acknowledgements support by R.O.C. MOST 104-2221-E-009-142-MY3 is acknowledged.

References

1. Rosensweig, R.E.: Ferrohydrodynamics. Cambridge University Press, Cambridge (1985) and references therein
2. Blums, E., Cebers, A., Maiorov, M.M.: Magnetic Fluids. De Gruyter, New York (1997) and references therein
3. Cowley, M.D., Rosensweig, R.E.: J. Fluid Mech. **30**, 671 (1967)
4. Friedrichs, R., Engel, A.: Phys. Rev. E **64**, 021406 (2001)
5. Chen, C.-Y., Cheng, Z.-Y.: Phys. Fluids E **20**, 054105 (2008)
6. Chen, C.-Y., Li, C.-S.: Phys. Fluids E **22**, 054105 (2010)
7. Chen, C.-Y., Wu, W.-L., Miranda, J.A.: Phys. Rev. E **82**, 056321 (2010)
8. Tsebers, A.O., Maiorov, M.M.: Magnetohydrodynamics (N.Y.) **16**, 21 (1980)

9. Langer, S.A., Goldstein, R.E., Jackson, D.P.: Phys. Rev. A **46**, 4894 (1992)
10. Jackson, D.P., Goldstein, R.E., Cebers, A.O.: Phys. Rev. E **50**, 298 (1994)
11. Pacitto, G., Flament, C., Bacri, J.-C., Widom, M.: Phys. Rev. E **62**, 7941 (2000)
12. Chen, C.-Y., Wu, H.-J.: Phys. Fluids **17**, 042101 (2005)
13. Wen, C.-Y., Chen, C.-Y., Kuan, D.-C.: Phys. Fluids **19**, 084101 (2007)
14. Saffman, P.G., Taylor, G.I.: Proc. R. Soc. Lond. Ser. A **245**, 312 (1958)
15. Chen, C.-Y., Tsai, W.-K., Miranda, J.A.: Phys. Rev. E **77**, 056306 (2008)
16. Miranda, J.A.: Phys. Rev. E **62**, 2985 (2000)
17. Chen, C.-Y., Wu, S.-Y., Miranda, J.A.: Phys. Rev. E **75**, 036310 (2007)
18. Dias, E., Miranda, J.A.: Phys. Rev. E **91**, 023020 (2015)
19. Cahn, J.W., Hilliard, J.E.: J. Chem. Phys. **28**, 258 (1958)
20. Lowengrub, J., Truskinovsky, L.: Proc. R. Soc. Lond. A **454**, 3617 (1998)
21. Lee, H.-G., Lowengrub, J., Goodman, J.: Phys. Fluids **14**, 492 (2002)
22. Lee, H.-G., Lowengrub, J., Goodman, J.: Phys. Fluids **14**, 514 (2002)
23. Chen, C.-Y., Huang, Y.-S., Miranda, J.A.: Phys. Rev E **84**, 046302 (2011)
24. Chen, C.-Y., Huang, Y.-S., Miranda, J. A.: Phys. Rev E **89**, 053006 (2014)
25. Huang, Y.-S., Chen, C.-Y.: Comput. Mech. **55**(2), 407–420 (2015)
26. Chen, C.-Y., Meiburg, E.: J. Fluid Mech. **371**, 233 (1998)
27. Ruith, M., Meiburg, E.: J. Fluid Mech. **420**, 225 (2000)
28. Meiburg, E., Chen, C.-Y.: SPE J. **5**, 2 (2000)